The Meteoritical Society

Meteoritics & Planetary Science 43, Nr 1/2, 75–86 (2008)
Abstract available online at http://meteoritics.org

Bulbous tracks arising from hypervelocity capture in aerogel

Josep M. TRIGO-RODRÍGUEZ[1, 2*], Gerardo DOMÍNGUEZ[3], Mark J. BURCHELL[4], Friedrich HÖRZ[5], and Jordi LLORCA[6]

[1]Institute Space Sciences–CSIC, Campus UAB, Facultat de Ciències, Torre C5-parell-2ª, 08193 Bellaterra, Barcelona, Spain
[2]Institut d'Estudis Espacials de Catalunya (IEEC), Edif. Nexus, c/Gran Capità, 2-4, 08034 Barcelona, Spain
[3]Department of Chemistry and Biochemistry, University of California, San Diego, La Jolla, California 92093, USA
[4]Centre for Astrophysics and Planetary Sciences, University of Kent, Canterbury, Kent CT2 7NH, UK
[5]LZ Technology Inc., ESC Group, JE23, 2224 Bay Area Blvd., Houston, Texas 77058, USA
[6]Institut de Tècniques Energètiques, Universitat Politècnica de Catalunya, Diagonal 647, ed. ETSEIB, 08028 Barcelona, Spain
*Corresponding author. E-mail: trigo@aliga.ieec.uab.es

(Submitted 23 March 2007; revision accepted 28 March 2008)

Abstract–The capture of 81P/Wild 2 cometary particles in aerogel with a well-defined impact velocity (6.1 km s^{-1}) has provided a wealth of data concerning the composition of Jupiter-family comets. To interpret this data we must understand the capture processes in the aerogel. A major category of tracks are those with bulbous cavities lined with particle fragments. We present a new model to account for the production of these "turnip"-shaped impact cavities. The model uses a thermodynamic approach in order to account for the likely expansion of vapors from particles rich in volatile species. Volume measurements of some of the largest Stardust tracks analysed so far, together with theoretical considerations, indicate that for the majority of Stardust cometary aggregate particle impacts, fragmentation of relatively weak impactors (combined with radial expansion of the resulting subgrains) is the leading cause of bulbous track production, while volatile release of vapors played a secondary role.

INTRODUCTION

Aerogels have been made from a variety of metal oxides since the 1930s, however their potential as a capture medium for hypervelocity cosmic dust is a relatively recent development (Tsou et al. 1988); see Burchell et al. (2006a) for a summary. The primary effect of such highly porous, low density materials is to reduce the shock stress upon impact to such an extent that the projectiles may survive hypervelocity collisions without excessive vaporization or melting. Due to its highly transparent nature, SiO_2-based aerogel was particularly suited for the Stardust mission (Tsou et al. 2003). In this paper we discuss the characteristics of some of these tracks and consider a model for their development.

Tracks in Stardust Aerogel

NASA's Stardust mission to comet 81P/Wild 2 employed as a cometary dust collector SiO_2-based aerogel having a continuous density gradient from 0.005 to 0.05 g/cm^3 over a target thickness of 3 cm; this collector was composed of 132 individual aerogel blocks, about 2 × 4 × 3 cm, and a total exposed surface of 1039 cm^2. Upon return, the initial inspection of the aerogel revealed a wide variety in track size and shapes (Hörz et al. 2006). These were analyzed and classified in detail by Burchell et al. (2008). In this initial survey and photographic documentation of tracks, each feature was labeled as follows: C2xxx-Ty, where C2 indicates it is the cometary (rather than interstellar) collector tray, xxx refers to the number and specific tray location of the aerogel tile, and y is the yth track found in that tile. Once extracted from a tile, each track receives a new permanent identifier in the form of a sequential number that reflects the chronological order in which individual tracks were processed. In this paper, where a track has been extracted we refer to it by the latter convention (i.e., Track x), otherwise we use the C2xxx-Ty convention.

Based on the study of the track images, three major morphologic types emerged: type A tracks—these were relatively long and narrow with captured grains near their end. Type B tracks (see Figs. 1 and 2)—these were bulbous immediately after the point of impact and grade to long, slender termini (there can be several termini in an impact feature) that individually resemble type A tracks. Type C tracks—these have bulbous cavities without a slender terminus. A detailed discussion of the frequency and morphology of each

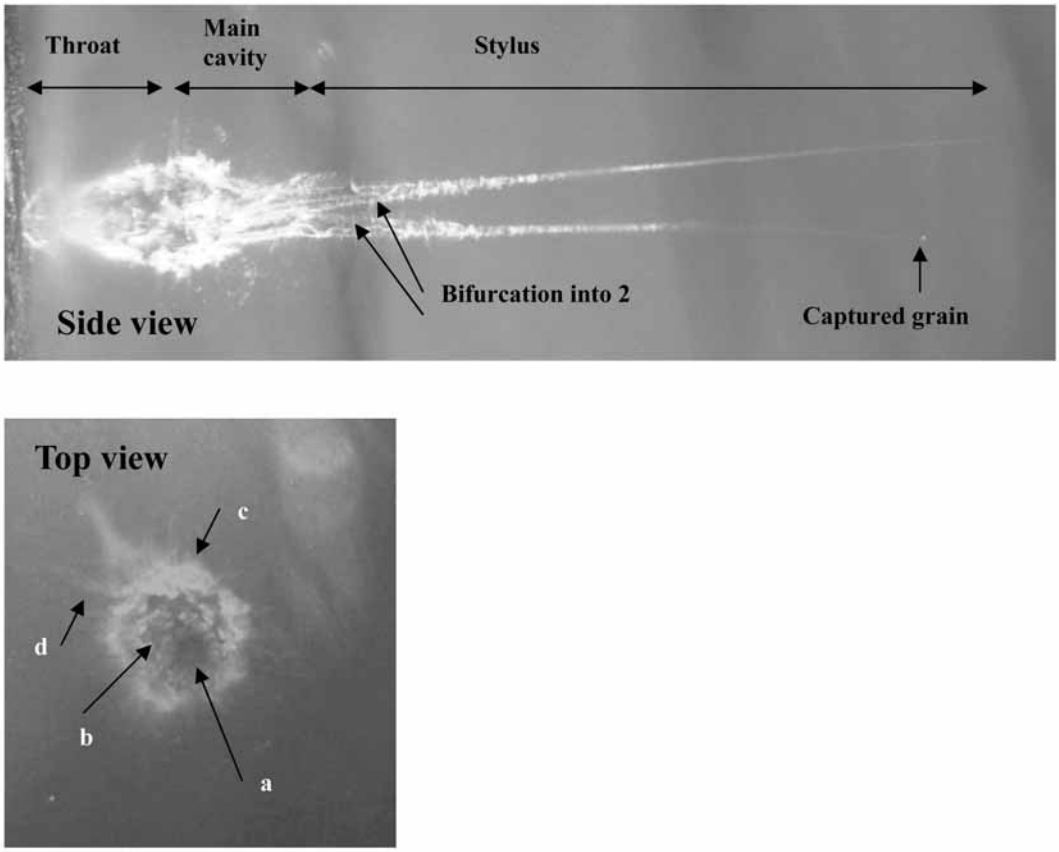

Fig. 1. Type B track with distinct track sections labeled as in the Hörz scheme. The track is about 1 cm long (Stardust C2126-T1). Top and side views are shown. In the side view (where the impact was from the left) as well as two subtracks opening beneath the main cavity, a subgrain is visible captured at the end of one subtrack. In the top view, the labeled parts are: a) track opening, b) surface depression around the track opening, c) subsurface widest extent of track, d) subsurface lateral fractures are just visible radiating from the cavity of the track.

type is given in Burchell et al. (2008). Here we note that type A comprised 65%, B 33%, and C 2% of all tracks. However, this split varies with track size; type B tracks dominate the long tracks, the domination becoming more pronounced as the track length increases.

A method of referring to the major morphological components of a track, e.g., cavity, styli etc. was developed by Hörz et al. (1998, 2000) and is illustrated on a Stardust track in Fig. 1. Also shown in Fig. 1 is a top view of the same track which shows a complex structure. There is an opening (entrance hole) into the interior of the aerogel (the track) which is surrounded by a depressed, and occasionally spalled region in the aerogel surface. Also, due to the transparency of the aerogel, subsurface features are visible although not fully in focus. Because the track cavity opens out to a larger diameter than the entrance hole, the subsurface track shows up in the top view with a larger diameter than the entrance hole and surface depression. Subsurface radial fractures in the aerogel can also be discerned. Another example of a type B track is shown in Fig. 2. Here as well as the bulbous main cavity and stylus beneath, there are small radial tracks emanating from the main cavity. There are what appear to be small (less than a few micrometer) particle fragments along these subsidiary, radial tracks. Thus some of the incident particle material has fragmented and been dispersed sideways along the length of the main track.

In the laboratory, projectiles with very different cohesive properties, composition and grain sizes reproduce the range of track morphologies as distinct classes (Hörz et al. 1998; Burchell et al. 2008). The Stardust aerogels contain the full range of these morphologies and their gradual transitions. The type A tracks are considered to be due to relatively strong, well condensed grains and in this paper are not considered further. Instead we focus on the type B (and type C) tracks which comprise the majority of the largest impact features in the aerogel (Burchell et al. 2008). Four tracks showing the range of morphologies for type B and C tracks are shown in Fig. 3. To better consider the main cavities that are distinctive of type B and C tracks see Fig. 4. In Fig. 4a the ratio of cavity length over total track length is plotted versus total track length. This indicates what fraction of the total track length is occupied by the cavity. For type B tracks the fraction of total track length taken up by the cavity ranges from 0.14 to 0.83, with an average of (0.53 ± 0.16). Thus typically the cavity extends half way down the total track. In Fig. 4b the bulbous nature of the cavity is indicated by plotting the maximum

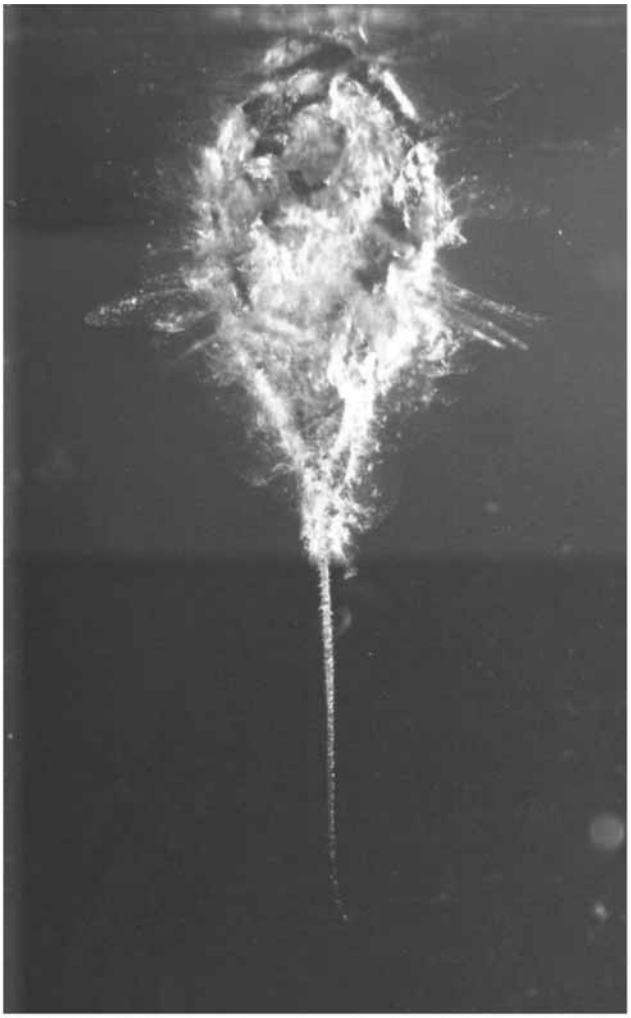

Fig. 2. Stardust Track 35 (impact was from the top of the image). This type B track clearly exhibits the lateral spreading of the materials after the entry and subsequent vaporization of the materials that produce the characteristic bulb. The hole diameter is 1480 μm, the greatest width of the bulb is 3530 mm and the track length is 1.17 cm. Note that the ending part resembles a type A track as consequence of the final deceleration of an ~50 μm mineral grain. (Image: Level 3 PET Stardust).

cavity width divided by cavity length. For type B tracks this ranges from 0.16 to 0.66, with a mean of (0.37 ± 0.11). For type C tracks the data in Fig. 4b tightly clusters around a mean of (0.39 ± 0.05). A width/length ratio for the cavity which tended to 0 would be a relatively long slender track, i.e., type A. Thus the lack of data at small values of this ratio is understandable. If the ratio tended to 1 a spherical cavity would be indicated, and if exceeding 1 would represent a squat prolate spheroid cavity (where the equatorial diameter is aligned with the track length). That the observed values of the ratio never approach 1 indicates that the axis of penetration, and thus impact direction, is more significant in determining overall cavity shape than is any sideways expansion of the cavity.

Laboratory impact experiments (e.g., Burchell et al. 2001, 2006a, 2006b) are usually limited to relatively dense and competent projectiles, such as glass or metal beads and carefully sized mineral fragments, all mostly producing type A tracks. Experiments with fragments of hydrated minerals, e.g., lizardite (Burchell et al. 2008) or compacted powders (Hörz et al. 1998) produced bulbous (type B or C) tracks. This suggests that some of the cometary particles may either be poorly cohesive, fluffy aggregates (which drive bulbous cavity expansion by radial motion of subparticles after disaggregation) or volatile-rich materials that produce energetic vapors (which in turn drive expansion of the bulbous cavities).

Given the relative invariant impact conditions during the comet encounter, such as a constant impact velocity of 6.1 km s^{-1} and impact angles normal to collector surface, the variety in track morphologies should directly reflect substantial variability in the physical/mineralogic/compositional properties of the cometary impactors. As a consequence, an improved understanding of the physics involved in the formation of aerogel tracks will assist determination of detailed properties of the original impactors. Laboratory experimentation, e.g., Noguchi et al. (2007) has shown that, dependent on the impactor properties, a variety of heating effects can occur during capture in aerogel, along with an intimate mixing of molten aerogel layers around the surfaces of captured grains. As well as observing molten aerogel, Noguchi et al. (2007) report effects on the captured particles which imply temperatures in excess of 500 °C for durations of order of a microsecond.

Analysis of the captured particles in the Stardust aerogel requires visual interpretation of captured terminal grains, subgrains along walls of tracks, imaging and elemental mapping of whole tracks, and analysis of the aerogel lining the walls of tracks, etc. (Brownlee et al. 2006; Zolensky et al. 2006; Sandford et al. 2006; Keller et al. 2006). An improved understanding of aerogel penetration and track formation, specifically of a projectile's pressure-temperature (hereafter PT) history, will thus greatly aid in determining possible alterations of the pristine comet particles by the capture process itself.

There has been previous work on understanding tracks in aerogel, but much of it has focused on the type A "carrot" shaped tracks. However, as stated earlier, in the returned Stardust collectors over 50% of tracks longer than 0.5 mm (corresponding to impactors larger than a few micrometres) are type B (Burchell et al. 2008). This is why we focus herein on type B track formation. In the next section a model is introduced that attempts to explain the bulbous type B tracks via the rapid, adiabatic expansion of vapors derived from volatile-bearing impactors. The degree to which this can adequately explain experimental observations is then discussed.

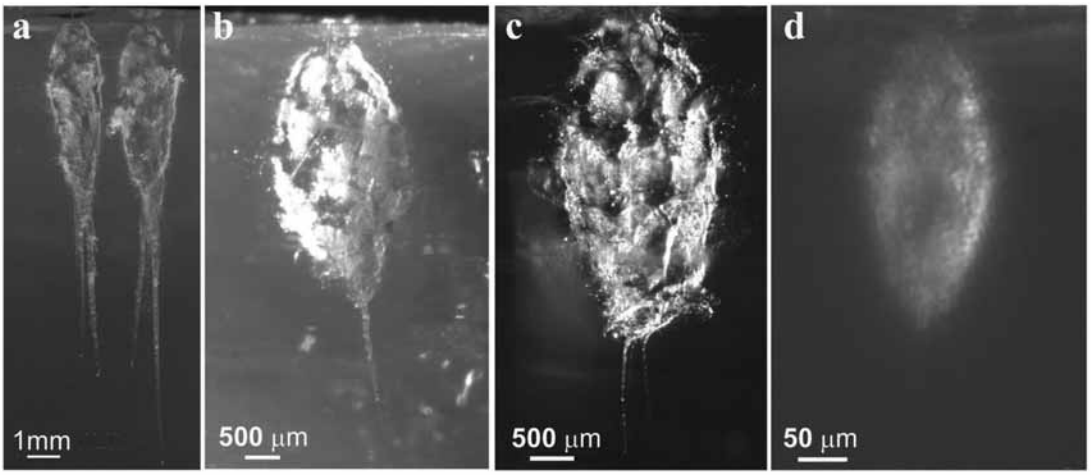

Fig. 3. Stardust tracks as imaged from the side (impacts were from the top of each image). Bulbous features are very prominent in all cases, but there is an apparent gradual transition from type B to C, suggesting that stylus formation depends of the size of the largest mineral grains that are embedded in the original particle. a) Track 32 (left) and 69 (right) are both good examples of large (8.5 and 11 mm, respectively) type B Stardust tracks with long stylus features. The other three tracks are much smaller, and they were labeled: b) C2086-T3 (type B), c) Track 80 (borderline type B/C), and d) C2052-T6 (type C). Track (d) is a small type C track without any discernible stylus features at the end (Images: Level 3 PET Stardust). Several of these images were also shown in Fig. 3 of Hörz et al. 2006.

Model of Hypervelocity Projectile Capture in Aerogel

We first give a simple description of the process that encapsulates the energetics of the penetration event into a porous material. Our approach follows that of Domínguez et al. (2004) and the reader is referred to that paper for a fuller discussion and derivation of the model (only directly relevant terms are given here). For simplicity of discussion, we will consider a spherical, single grained projectile (with drag coefficient equal to one), although it should be noted that these general principles can also be applied to non-spherical projectiles.

The energy required to deform, heat, and vaporize both the aerogel target and the projectile is derived from the kinetic energy of the projectile. Assuming that all the kinetic energy is coupled back into the projectile upon impact, the fraction of the projectile that *could* potentially be vaporized is given by:

$$\frac{m_{vap}}{m_g} = \frac{v_0^2}{2H_{vap}} \quad (1)$$

where H_{vap} is the specific heat of vaporization of the projectile material, v_0 is the impact velocity of the projectile and m_g is the mass of the projectile. Figure 5 shows the degree of vaporization as a function of incident speed for materials such as water and olivine, with H_{vap} of 2.26 and 19.52 MJ kg^{-1} respectively. In the best case shown (forsterite), for impacts with v just above 6 km s^{-1}, the kinetic energy (if completely coupled back into the projectile as heat) would be sufficient to vaporize the projectile. How then do hypervelocity projectiles survive the capture process? Not all the kinetic energy is coupled back in to the particle; some is partitioned into the target and ~50% of the total kinetic energy, for high impact velocities, is typically converted into thermal energy (e.g., Melosh 1989). More importantly, the use of aerogel significantly decreases the shock pressure, which in turn reduces projectile heating.

To gain some intuition about the magnitude of the deceleration force, time scale, and stopping length of a projectile with radius r_g, in an aerogel collector with density ρ_0, it is useful to view the capture process from the projectile's point of view. In this frame, a projectile of radius r_g sees a mass flux (Φ_m), a momentum flux (Φ_{mv}), and a kinetic energy flux (Φ_{KE}) given by:

$$\Phi_m = \rho_0 \pi r_g^2 v \quad (2)$$

$$\Phi_{mv} = \rho_0 \pi r_g^2 v^2 \quad (3)$$

$$\Phi_{KE} = \frac{1}{2}\rho_0 \pi r_g^2 v^3 \quad (4)$$

Of particular interest are the momentum and kinetic energy fluxes, since these quantities have units of force (*dp/dt*) and power (*dE/dt*). These ultimately determine the momentum loss of the projectile and the energy available to heat the projectile.

To an order of magnitude the deceleration force experienced by the projectile is:

$$\frac{dp}{dt} \approx \rho_0 A v^2 \quad (5)$$

where A is the cross sectional area of the projectile (similar to Kadono 1999 and Domínguez et al. 2004 if the crushing strength of the material is negligible and the drag coefficient

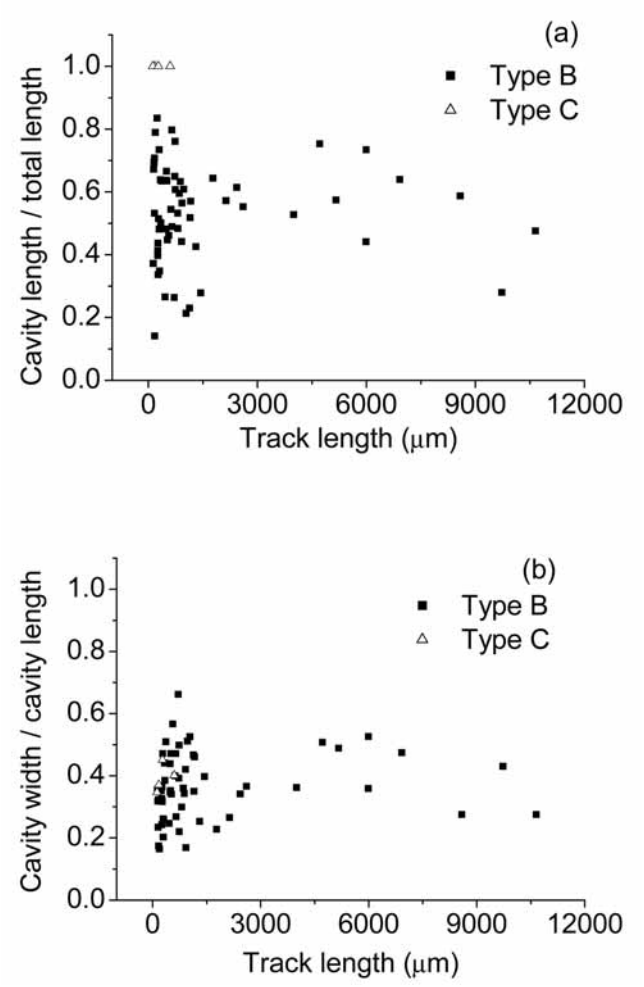

Fig. 4. Stardust type B and C tracks. a) The fractional length of the cavity compared to the total track length. b) The ratio of cavity width to cavity length. Both are plotted against total track length.

is not explicitly stated with its variation with speed contributing to the overall uncertainty in the approximation). The dynamic pressure felt by the projectile can be estimated by considering the force per unit area experienced by the projectile, given by:

$$P \approx \rho_0 v^2 \tag{6}$$

The capture-length scale (λ) can be shown (Domínguez et al. 2004) to be given by:

$$\lambda \approx \frac{4}{3}\left(\frac{\rho_g}{\rho_0}\right) r_g \tag{7}$$

These estimates are in good agreement (to order of magnitude) with experimental observations of the relationship between the length of tracks and the ratio of projectile to aerogel density (Domínguez et al. 2004).

The time scale for capture can be estimated by calculating the ratio of initial momentum to the rate of momentum flux seen by the projectile (density ρ_g), which is given by:

$$\tau = \frac{\rho_0}{\Phi_p} = \frac{4}{3} r_g \left(\frac{\rho_g}{\rho_0}\right) \frac{1}{v_0} \tag{8}$$

This time scale is sensitive to the ratio of projectile to aerogel density and effectively spreads the heating over longer time scales. There is little direct data on capture time scales to compare Equation 8 to. However, Noguchi et al. (2007) estimate, based on observed mineralogical changes in impacts at 6.18 km s^{-1} of serpentine grains (30 μm in diameter, size estimated from an image in their paper) captured in aerogel (density 30 kg m^{-3}), a heat pulse of 1 to 1.8 μs duration. Based on Equation 8, a capture time scale of approximately 0.3 μs is predicted, within a factor of 10 of the heat pulse duration. Since aerogel is a poor heat conductor, the heat pulse time scale is longer than the capture time scale by a factor determined by the radiative heat loss rate.

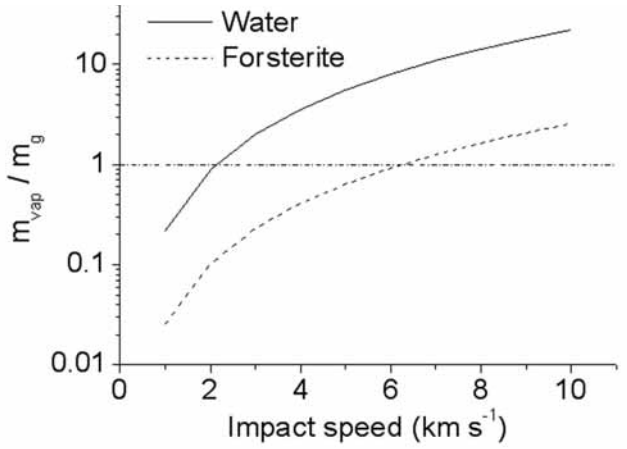

Fig. 5. Fraction of mass of incident particle vaporized by impact (see Equation 1).

Capture in low-density polymer foams was addressed analytically by Anderson and Ahrens 1994 and subsequently applied to aerogels (Anderson 1998) (similarities exist with the detailed treatment that Öpik 1958 gave to the problem of meteoroid entry into the atmosphere). The Anderson and Ahrens model used a combination of aero drag, viscosity of the foam and ablation of the impactor to stop penetration of the particle into the target medium, although projectile disaggregation/fragmentation and/or volatile driven projectile disruption were not specifically addressed.

Generally calculations of shock pressure experienced by a projectile are most accurate when they are based on empirically determined equations of state including shock Hugoniots (e.g., relationships between shock velocity U and particle speed u_p), simple descriptions of porous solids as "ideal-compressible solid" or "locking solid" can be used as a first approach to the shock velocities and shock pressures of

these materials. In this framework, the solid (of density ρ_0) is described as consisting of a porous network of solid particles (of density ρ_1) which, when subjected to high shock pressures, collapses to yield a high density solid of density ρ_1 (Zeldovich et al. 1966; Trucano and Grady 1995). The compressibility of the material (k) is the only parameter necessary to describe the solid in the strong shock limit and this compressibility factor is defined as:

$$k = 1 - (\rho_0/\rho_1) \tag{9}$$

Applying this model to the first Hugoniot equation gives:

$$U = \frac{u_p}{k} \tag{10}$$

where U is the shock velocity and u_p is the particle velocity. This result implies that locking solids are expected to have polynomial shock Hugoniots

$$U = C_0 + su_p + s'u_p^2 \tag{11}$$

with parameters $C_0 = 0$, $s = 1/k$, and conveniently s' and s" = 0, comparable to the frequently used linear shock equations where C_0 and s are finite with no higher order terms. In Fig. 6 the shock pressure calculated from the locking solid model for a particle impacting an aerogel of density 20 mg/cc is shown vs. particle velocity. The value of k used (k = 0.992) was obtained assuming that the maximum shocked density of aerogel is the density if it were non-porous (approximately 2500 mg/cc). For comparison the shock pressure calculated using the shock Hugoniot data of Anderson 1998 (which provides empirical relationships for C_0 and s) is also shown in Fig. 6; there is a slight step in the predicted shock pressures at 4 km s^{-1} as there are different relationships for C_0 and s above and below this speed. In general there is good agreement in the estimated shock pressures from both methods for impact speeds in the km s^{-1} range. For completeness we also show on Fig. 6 the crushing strength of aerogel (density 20 mg/cc) estimated using the results of Domínguez et al. (2004). For impact speeds above 1 km s^{-1}, the crushing strength of such aerogel (12.4 kPa) can be seen to be several orders of magnitude less than the estimated shock pressures.

In the locking solid approximation, when $\rho_1 >> \rho_0$, the second and third Hugoniot equations can be reduced to

$$P_1 - P_0 = \rho_0 u_p^2 \tag{12}$$

and

$$E_1 - E_0 \cong \frac{u_p^2}{2} \tag{13}$$

In the absence of phase changes, this change in internal energy is equal to the enthalpy change of the solid and can be used to estimate the temperature of the shocked material if the heat capacity of the material is known. In addition, the internal energy gained by the newly shocked material is given by:

$$\Delta E_k = \frac{u_p^2}{2} \tag{14}$$

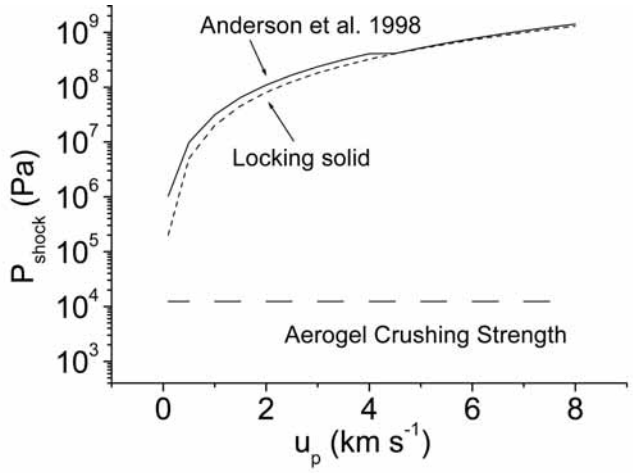

Fig. 6. Comparison of empirical shock pressures derived from Anderson et al. (1998) and shock pressures predicted by the locking solid model (k = 0.992) versus impact speed for 20 mg/cc aerogel. See text for details. For comparison, the estimated crushing pressure of 20 mg/cc aerogel is shown which is obtained from Equation 18 in Domínguez et al. (2004).

In the strong shock limit, there is an equipartition between the kinetic and internal energy that is transmitted to a fluid element. The validity of these approximations for low-density solids was examined experimentally and computationally by Trucano and Grady (1995). In particular, Trucano and Grady (1995) found that the deceleration of solid copper spheres (initial speeds in the range 2–4 km s^{-1}) in hydrocarbon foam (density 176 kg m^{-3}) was well described by a hydrodynamic deceleration of the form:

$$m\frac{du}{dt} = \frac{1}{2}\rho_0\left(\frac{1+k}{2}\right)v^2 A_{eff} \tag{15}$$

where k is once again the compressibility of the target and A_{eff} is the fraction of the geometric cross section that experiences a deceleration pressure equal to $(1/2)\rho_0 v^2$. Note the similarity to the simple estimate given by Equation 5.

Adopting the simplified locking solid framework permits a derivation of analytic expressions for the velocity and kinetic energy of captured spherical grains as:

$$v(z) = v_i e^{-z/2\lambda} \tag{16}$$

Table 1. The entrance hole diameter (*EHD*) and the original particle diameter (*OPD*) are given for the largest tracks studied. From the EHD, the original particle size was obtained by using Equation 6 derived by Burchell et al. (2008). *K* refers to the available kinetic energy at the point where the bulb-like feature reaches its maximum width (computed using Domínguez et al. 2004 model). Such energy is compared to the estimated adiabatic work of the expansion (W_{adi}) obtained from Equation 23.

Track no.	EHD (μm)	OPD (μm)	V_e ($\times 10^{10}$ μm^3)	K ($\times 10^6$ ergs)	W_{adi} ($\times 10^6$ ergs)
C2054_T3	700 ± 10	106 ± 13	2.2 ± 0.2	3.2 ± 0.4	1.1 ± 0.4
C2027_T6	370 ± 10	75 ± 12	0.3 ± 0.1	2.6 ± 0.3	0.4 ± 0.2
C2027_T7	350 ± 10	72 ± 12	0.3 ± 0.1	2.5 ± 0.3	0.4 ± 0.2

and

$$E(z) = E_0 e^{-z/2\lambda} \tag{17}$$

respectively (Kitazawa et al. 1999; Domínguez et al. 2004). These expressions, while derived for spherical grains, are adequate representations of the deceleration profiles for irregular objects and are accurate to within a factor of 2. They will be used as a baseline in discussions on the relative roles of projectile fragmentation and volatiles in the track formation processes.

In the Domínguez et al. (2004) model, half of the kinetic energy loss of the projectile was transferred to the aerogel directly encountered by the projectile, essentially pushing the compressed aerogel outwards with a velocity that is comparable to the velocity of the projectile. The other half of the projectile's energy loss per unit length was coupled into heating the compressed aerogel. Near the surface of the aerogel, the resulting shock wave resembles a spherical explosion while away from the surface, it takes on a conical geometry. Using a locking solid formalism and the Hugoniot equations, the model found the attenuation of the shock wave's ram pressure ($\sim\rho_0 v_s^2$) to scale as r^{-4}. In this approach, the final size of the impact track was determined by setting the ram pressure equal to the crushing strength of the aerogel.

In contrast, Kadono (1999) proposed a model of impact crater formation in low density foams where all of the energy loss of the projectile was coupled entirely into the target as heat. The hot vapor cloud then transferred its heat to the emerging walls of the target, producing additional vapor and enlarging the cavity. This process continued until a thermodynamic equilibrium was reached. When this mechanism is applied to aerogels, a simple estimate of the energy required to vaporize SiO_2 indicates that aerogel is energetically expensive and by itself cannot be the dominant mechanism that accounts for the size of bulbous impact cavities observed in aerogels (Domínguez et al. 2004).

Application to Cometary Dust Capture and Track Formation

As described above, the modeling work done until now has mainly focused on the track formation resulting from the capture of solid, mechanically strong projectiles in the laboratory (i.e., type A tracks). Many of the cometary dust grains captured by Stardust undoubtedly do not fall into this category, as they are likely to be highly porous, organic-rich loose aggregates (Zolensky et al. 2006; Hörz et al. 2006; Sandford et al. 2006; Keller et al. 2006). There is a lack of experimental data on impact cratering of this kind of projectiles since they are too fragile for surviving the rapid accelerations used in light-gas gun and plasma gun facilities. This status poses difficulties for modelers attempting to explain the type B and C "bulbous" tracks seen in the Stardust cometary dust collection. However, what is known about the physics of impact track formation in aerogels permits placing some quantitative constraints on the sensitivity of the track formation process to projectile fragmentation and/or volatile vapor production. To this end an adiabatic expansion model is developed here for impacts by volatile rich projectiles.

In the simplest treatment, the formation of a bulbous cavity can be explained as resulting from the adiabatic expansion of a hot vapor plume. This vapor could arise from the heating of the target material (e.g., see Kadono 1999). Here we consider the case that the vapor is produced by the capture of a volatile-rich projectile. In this model, the mechanical strength of the aerogel is largely neglected and is used only to establish the boundary condition where the growth of the track can no longer proceed. In this model, the initial and final track volumes are related by:

$$T_0 V_0^{\gamma - 1} = T_e V_e^{\gamma - 1} \tag{18}$$

where γ is the adiabatic constant for the vapor cloud. As a rough approach, we assume that the original volume (V_0) is equal to that of the particle and that the maximum temperature reached is about 2000 K (for melted SiO_2). In this model, the energy required to excavate a track volume (V_e) can be estimated by assuming that the vapor is an ideal gas giving:

$$W_{ad} = \frac{P_0 V_0 - P_e V_e}{\gamma - 1} \tag{19}$$

Comparisons of the work done with the available kinetic energy at a given depth show that this model is consistent within an order of magnitude with observations. The main properties of the largest type B tracks are used for testing this

model, particularly the entrance hole diameter, and the volume excavated in the aerogel. Experimental results are compared with the predictions of this model in Table 1. The work done by the expansion of vapors is about one-fifth of the available kinetic energy.

The contribution of released vapors to tracks' excavation can be also addressed by using a theoretical approach. The initial size of the track is set by the size of the projectile, the energy loss of the projectile establishes an energy density, or equivalently, a pressure. The Domínguez et. al. (2004) model assumed that half the kinetic energy loss of the projectile was transferred to the aerogel as kinetic energy, leading to a kinetic pressure (snowplow) wave of shock compressed aerogel in front and to the side of the penetrating particle. The other half of the energy contributes to the thermal pressure of vapor products produced along the projectile trajectory, but these were then neglected in that model. We assume that a fraction, f_E, is directly coupled into the thermal energy of the vapor within the cloud. In this case, an upper limit to the thermodynamic pressure is given is by:

$$P_T \cong f_E\left(\frac{dE}{dz}\right)\left(\frac{1}{\pi \cdot r_g^2}\right) \tag{20}$$

which simplifies to:

$$P_T \approx \left(\frac{f_E}{2}\right)\rho_0 v^2 \tag{21}$$

when we adopt the simple exponential form for the kinetic energy of Equation 17. Equation 21, however, ignores the energy expended in producing the vapor cloud and is an upper limit to the thermodynamic pressure that the vapor cloud can have. A refinement on Equation 21 can be derived by considering the amount of energy per unit mass, needed to raise the temperature of the aerogel to the vaporization temperature ($C_p\Delta T$) and the energy expended in vaporizing a fraction of the aerogel. When these are considered, the thermodynamic pressure of this vapor cloud is given by:

$$P_T \approx \rho_0 v^2\left[f_E - \frac{(C_p\Delta T) + f_v H_v}{v^2}\right] \tag{22}$$

where f_v is the fraction of aerogel, per unit length, that is vaporized, H_v is the heat of vaporization for silica, and $C_p \cdot \Delta T$ is the energy required to raise the temperature of 1 kg of aerogel to the vaporization point and v^2 is the velocity of the projectile. It should be noted that C_p is the average heat capacity of silica over the range ΔT. For typical values of C_p for silica at room temperature (~700 J kg^{-1} K^{-1}), this energy represents only a fraction (<5%) of the energy required to vaporize the aerogel (ΔT ~ 2000 K, H_v ~ 33.6 × 10^6 J kg^{-1}). Ignoring the $C_p\Delta T$ term, we find that the thermodynamic pressure along the track is given approximately by:

$$P_T = \left(\frac{\rho_0}{2}\right)v^2\left[f_E - f_v\left(\frac{5.6}{v}\right)^2\right] \tag{23}$$

where v is the projectile's velocity in km/s.

The pressure (thermal or kinetic) is independent of the size of the projectile. The size of the projectile and its possible fragmentation, however, is important for determining the final size of the cavity as it establishes the initial boundary conditions for the pressure pulse duration. The final size of the cavity is determined by the attenuation of the pressure acting on the aerogel (either the kinetic ram pressure P_k or, in the vapor model, the thermal pressure P_T) as the vapor cloud pushes the aerogel out. The Domínguez et al. model of track formation argued that this attenuation scales as:

$$P_k(r) \approx \frac{\rho_0}{2}v^2\left(\frac{r_g}{r}\right)^4 \tag{24}$$

and in the adiabatic expansion model one expects this attenuation to be given approximately by:

$$P(r) = P_T\left(\frac{r_g}{r}\right)^{2\gamma} \tag{25}$$

Assuming that the vapor is an ideal gas ($\gamma = 5/3$) gives the power dependence on r as 10/3 which is not as steep as the Domínguez et al. model. Consequently, the pressure generated by hot vapors released should have a minor contribution in track excavation, as also suggested by the experimental data (Table 1).

DISCUSSION

The "bulbous" type B and C tracks seen in Stardust have, for a given entry hole size, diameters that are larger than those expected for solid grains in laboratory experiments implying that the rate of energy deposition during the capture process has deviated significantly from what is found from solid single-grain projectiles in the laboratory. The preliminary examination of the returned Stardust aerogel samples found that projectile fragmentation was ubiquitous during the capture of comet Wild 2 particles (Hörz et al. 2006; Burchell et al. 2008) but also found that the capture process produced significant amounts of fine-grained deposits along the walls of tracks (see e.g., Flynn et al. 2006; Sandford et al. 2006). Zolensky et al. (2006) proposed a structural model of weakly constructed mixtures of nanometer-scale grains with occasionally larger (>1 μm) mineral grains. Such particles, especially those having a "fluffy" structure, from 81P/Wild 2 have important implications in the excavation of Stardust's tracks, particularly with regard to the production of bulbous

features by the likely two main processes: 1) fragmentation and 2) volatile release.

To determine the relative role of each of these we have developed the following approach. We can use the shock pressure attenuation expressions discussed in the previous section. For both the snowplow and adiabatic expansion models, we expect that the tracks scale as:

$$r_T \approx r'_g \left(\frac{P_T}{P_c}\right)^{\alpha} \tag{26}$$

where r'_g is the effective radius of the initial volume with pressure P_T, P_c is the crushing strength of the aerogel. The initial pressure falls off as radius grows with power $\alpha = ¼$ or 3/10 in the Domínguez and adiabatic models, respectively (see above). The scale at which cavity growth is effectively halted is when the pressure no longer exceeds the crushing pressure of the aerogel. The final track size is sensitive to the size of the projectile, but weakly dependent on the pressure. To illustrate the consequences of this, consider a bulbous track whose maximum diameter is a factor of X larger than what would be expected for the standard type A track of a given size of the entry hole and associated laboratory calibrations with spherical glass beads of radius r_g. The increased diameter of this track implies that either a) the effective size of the projectile increased by a factor of $r'_g \sim Xr_g$ or b) that the release of cometary volatiles increased P'_T by a factor of $X^{1/\alpha}$, or equivalently that:

$$P_T \approx P_0 X^{1/\alpha} \tag{27}$$

We next consider the two scenarios that are currently proposed as candidates for the production of bulbous tracks in aerogel.

Projectile Breakup

Evidence of broken up cometary dust grains is abundant in the Stardust cometary dust samples (Hörz et al. 2006). Initially on impact, kinetic energy is transferred to the shock front that increases its temperature sufficient to melt the aerogel. Once the particle penetrates into the aerogel, the dynamic pressure ($\sim\rho_0 v^2 \approx 300$ MPa) exceeds the particle's dynamic strength, and the particle breaks up. Recent studies on the fragmentation of cometary meteoroids reaching the Earth's atmosphere show that these particles have typical dynamic tensile strengths of ~10 kPa (Trigo-Rodríguez and Llorca 2006, 2007). Given this low strength, cometary grains would deform and break up rapidly upon impact on aerogel and as a consequence, the amount of energy deposited per unit track length increases as the effective size of the projectile increases due to flattening and lateral dispersion. In the Stardust data, type A, "carrot" shaped tracks were found to have width/total length ratios of approximately 0.05 to 0.11, whereas type B, "turnip" shaped tracks possessed ratios of 0.11 to 0.35 (Burchell et al. 2008). A type B track therefore has a width/length ratio typically some 2–3 times that expected for type A tracks. A bulbous track, whose dimensions indicated that $X \sim 2$ for example, would need a corresponding increase in the effective size of the projectile. This spreading would lead to large variations in the amount of capture heating experienced by the individual dust grain fragments found within a given impact (see Fig. 7).

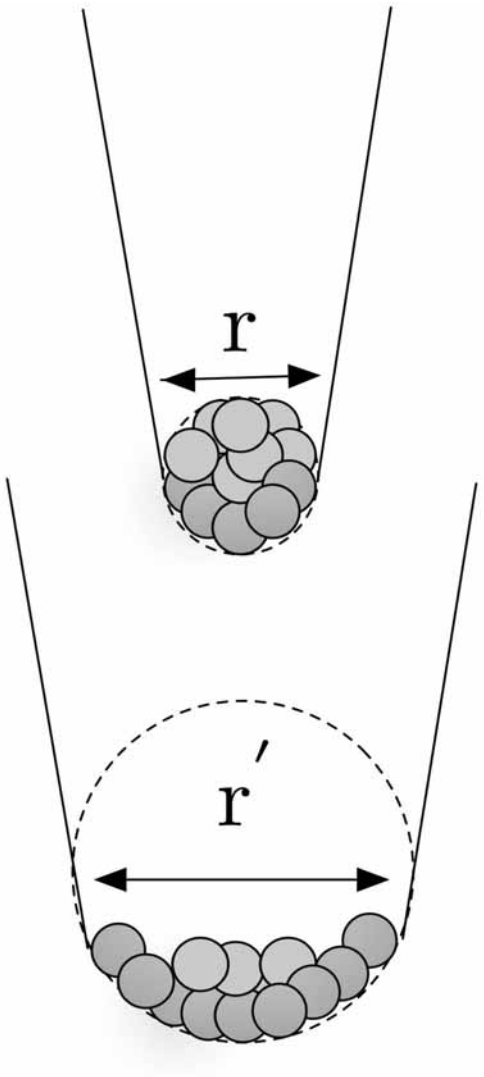

Fig. 7. Simplified model of dust aggregate consisting in components of similar size. Projectile fragmentation and shock front scale lengths. The projectile below has the same mass but has fragmented, resulting in a larger effective size and corresponding energy deposition, which is ultimately reflected in the track radius. Ablation of those materials located behind can be prevented by shielding.

Volatile Release

For a bulbous track where $X \sim 2$, the above analysis and current models of impact track scaling imply that the additional pressure required to produce these bulbous cavities

is on the order of 2^4 (snowplow model) and $2^{10/3}$ (adiabatic model) times the pressure produced by a solid, rigid projectile. To be general, we keep X variable and use this energetic requirement to constrain the composition of the vapor cloud that produces the bulbs observed in type B and C tracks (Burchell et al. 2008). This additional pressure requirement can be expressed as:

$$P'_T = P_T X^{1/\alpha} \tag{28}$$

If the vapor cloud that is responsible for this additional expansion is assumed to be an ideal gas, then:

$$P'_T \left(\frac{\rho_{vap}}{M}\right) kT_{vap} \tag{29}$$

where the sub index "vap" refers to vapor. Setting the above two equations and solving for ρ_{vap} gives us:

$$\rho_{vap} \approx 647 \text{kg m}^{-3} \left(\frac{X}{2}\right)^{3/10\alpha} \times \frac{M}{30\ a.m.u.} \left(\frac{\rho_0}{20}\right) \left(\frac{v}{6 \times 10^3 \text{m s}^{-1}}\right)^2 \left(\frac{2000}{T_{vap}}\right) \tag{30}$$

where M is the molecular weight and ρ_0 units are in kg m^{-3}.

It is important to note that this is the mass density of the vapor cloud that is required immediately after the passage of the projectile. This volume is approximately given by the volume of the projectile itself, and thus the fraction of the projectile mass per unit length that would need to be vaporized to produce a track with a cavity a factor of two wider than the size produced by a solid non-volatile laboratory projectile is given by:

$$\%_{vaporized} = 100 \times \frac{\rho_{vap}}{\rho_{projectile}} \approx 100 \times \frac{647 \text{kg m}^{-3}}{\rho_{projectile}} \tag{31}$$

Thus, we find that the energetic requirement to produce the bulbous tracks requires that a significant fraction of the projectile mass would be needed to provide the additional energy. For example, if a typical density were taken as 2500 kg m^{-3}, the $\%_{vaporized}$ would have to be some 26% of the original material per unit length. Even if the vapor cloud temperature is assumed to be as high as 10^4 K, the fraction of the projectile mass required to sustain these pressures is quite high.

Although both processes described above presumably participated in track formation, particle break-up seems to be the main source of additional energy required for explaining the observed deviations in hole diameters and track volumes from type A, "carrot" shaped tracks (Burchell et al. 2008). This seems consistent also with the observation that projectile fragments are found in bulbous cavities in considerable amounts, including the small-scale tracks that radiate from the main cavity.

How the Bulbous Tracks then Develop into Their Final Appearance

Once the disaggregation of the incident particle has occurred, the final bulbous shape tracks emerge (type B and C Stardust tracks). The almost instantaneous fracture of the aggregated particles increased the size of the bow-shock front leading to a track dimension that was also proportionally larger. Generation of ablation vapors of low-melting phases (like e.g., a CHON component) and fine-dust materials increased the size of the shock front to some extent, but as indicated above, was probably a secondary effect. When ablation of the front materials was almost complete, the bowl-shaped head dissipated, and consequently some of the heat of the thermal wave could propagate backwards, vaporizing the volatile phases present in the subgrains located behind the front-runners. This can also explain the transition between the main cavity and the bifurcations excavated by solid components surviving the initial phase (Fig. 1). Outward expansion of released gases throws small particles sideways, lining the walls of cavities with fine grained material and may also create the visible radial features in tracks which contain discrete subgrains of the impactor (e.g., Track C2054-T3, Fig. 2). If these small subgrains were behind the initial shock they may contain residues which have been removed from the front running grains by thermal effects. Flynn et al. (2006) found that mapping elements along a whole track showed that the terminal grain at its end had a different relative elemental composition to the subgrains, with the moderately volatile elements preferentially found distributed along the track rather than in the terminal grain, suggestive of processing during capture in a fashion giving selection effects on what material is observed where.

Self-shielding of fragments took place to some degree along the whole length of tracks. Shielding is beautifully exemplified in Fig. 2 of Brownlee et al. (2006) where a terminal particle *T57 Febo* (clearly not exhibiting rotation probably due to the continuous effect of viscosity during its capture) has been preserved behind an aggregate of fine-grained materials with approximately chondritic elemental composition, but also containing slightly heated carbonaceous materials and a pronounced enrichment in $^{15}N/^{14}N$ of unequivocal cometary origin (Matrajt et al. 2007). Shielding would also provide a natural explanation to the survival of organics deep into Stardust's tracks (Sandford et al. 2006). In parallel to this shielding by disaggregation, there is also evidence for ablation of surface material from grains (mixed with molten aerogel). This ablation will remove heat from grains, again exposing fresh, relatively unaltered material late during the capture phase and near the end of tracks.

CONCLUSIONS AND FUTURE WORK

In this paper, the formation of bulbous shaped tracks in aerogels has been considered. The carrot-shaped tracks often

reported in laboratory experiments (e.g., see Burchell et al. 2006 for a review) are held to arise from relatively intact survival of relatively strong well consolidated grains where a large fraction of the incident particle is retained as a single grain at the end of the track. By contrast, bulbous tracks distribute the bulk of the incident material along the main cavity. Two mechanisms for this have been considered, disaggregation due to low strength and volatile driven disaggregation under thermal heating and adiabatic expansion. The former is shown to be a strong candidate as the cause of disruption if particle strengths are weak as suggested by meteoroid studies. However, volatile expansion effects are non-negligible and while not dominant, could also play a role in the formation of bulbous Stardust tracks.

It would be interesting to test disaggregation in laboratory simulations using two stage light-gas guns. However, weakly bound aggregates are by definition not able to survive the shock of acceleration during the launch phase in light gas guns, making such studies difficult. Similarly, many volatile rich samples used in light-gas gun studies thus far turn out on examination to be heavily fractured pre-shot and are thus not good analogues for these studies. Ongoing work may ameliorate both these problems.

Composition studies of individual grains and subgrains captured by Stardust are been widely carried out. To understand the relation of these observations to the original pre-impact dust an understanding of the mechanisms of aerogel track formation and how they affect the grains is required (as given here for type B tracks). It is this synthesis of results which will reveal the true subtle nature of comet 81P/Wild 2.

Acknowledgments—We thank the Stardust mission leaders and the Johnson Space Center Curatorial Staff for providing us with the images and access to the data presented herein. We thank W. Anderson (LANL) and P. Tsou (JPL) for helpful conversations and comments. The referees are thanked for their helpful suggestions. Finally, JMT-R thanks Ministerio de Educación y Ciencia (MEC) for a JdC research grant and Consejo Superior de Investigaciones Científicas (CSIC) for a JAE-Doc grant. G. D. would like to acknowledge the support of NASA grant NNOXO7AM66G.

Editorial Handling—Dr. Marc Caffee

REFERENCES

Anderson W. W. and Ahrens T. J. 1994. Physics of interplanetary dust capture via impact into organic polymer foams. *Journal of Geophysical Research* 99:2063–2071.

Anderson W. W. 1998. Physics of interplanetary dust collection with aerogel. NASA STI/Recon Technical Report NASACR-1998-207766.

Brownlee D., Tsou P., Aléon J., Alexander C. M. O'D., Araki T., Bajt S., Baratta G. A., Bastien R., Bland P., Bleuet P., Borg J., Bradley J. P., Brearley A., Brenker F., Brennan S., Bridges J. C. Browning N., Brucato J. R., Brucato H., Bullock E., Burchell M. J., Busemann H., Butterworth A., Chaussidon M., Cheuvront A., Chi M., Cintala M. J, Clark B. C., Clemett S. J., Cody G., Colangeli L., Cooper G., Cordier P. G., Daghlian, C., Dai Z., D'Hendecourt L., Djouadi Z., Dominguez G., Duxbury T., Dworkin J. P., Ebel D., Economou T. E., Fairey S. A. J., Fallon S., Ferrini G., Ferroir T., Fleckenstein H., Floss C., Flynn G., Franchi I. A., Fries M., Gainsforth Z., Gallien J.-P., Genge M., Gilles M. K., Gillet P., Gilmour J., Glavin D. P., Gounelle M., Grady M. M., Graham G. A., Grant P. G., Green S. F., Grossemy F., Grossman L., Grossman J., Guan Y., Hagiya K., Harvey R., Heck P., Herzog G. F., Hoppe P., Hörz F., Huth J., Hutcheon I. D., Ishii H., Ito M., Jacob D., Jacobsen C., Jacobsen S., Joswiak D., Kearsley A. T., Keller L., Khodja H., Kilcoyne A. L. D., Kissel J., Krot A., Langenhorst F., Lanzirotti A., Le L., Leshin L., Leitner J., Lemelle L., Leroux H., Liu M.-C., Luening K., Lyon I., MacPherson G., Marcus M. A., Marhas K., Matrajt G., Meibom A., Mennella V., Messenger K., Mikouchi T., Mostefaoui S., Nakamura T., Nakano T., Newville M., Nittler L. R., Ohnishi I., Ohsumi K., Okudaira K., Papanastassiou D. A., Palma R., Palumbo M. O., Pepin R. E., Perkins D., Perronnet M., Pianetta P., Rao W., Rietmeijer F., Robert F., Rost D., Rotundi A., Ryan R., Sandford S. A., Schwandt C. S., See T. H., Schlutter D., Sheffield-Parker J. A., Simionovici S., Sitnitsky S. I., Snead C. J., Spencer M. K., Stadermann F. J., Steele A., Stephan T., Stroud R., Susini J.,. Sutton S. R., Taheri M., Taylor S., Teslich N., Tomeoka K., Tomioka N., Toppani A., Trigo-Rodríguez J. M., Troadec D., Tsuchiyama A., Tuzolino A. J., Tyliszczak T., Uesugi K., Velbel M., Vellenga J., Vicenzi E., Vincze L., Warren J., Weber I., Weisberg M., Westphal A. J., Wirick S., Wooden D., Wopenka B., Wozniakiewicz P. A., Wright I., Yabuta H., Yano H., Young E. D., Zare R. N., Zega T., Ziegler K., Zimmerman L., Zinner E., and Zolensky M. 2006. Comet Wild 2 under a microscope. *Science* 314:1711–1716.

Burchell M. J., Thomson R., and Yano H. 1999. Capture of hypervelocity particles in aerogel: In ground laboratory and low Earth orbit. *Planetary and Space Science* 47:189–204.

Burchell M. J., Creighton J. A., Cole M. J., Mann J., and Kearsley A. T. 2001. Capture of particles in hypervelocity impacts in aerogel. *Meteoritics & Planetary Science* 36:209–221.

Burchell M. J., Graham G., and Kearsley A. 2006a. Cosmic dust collection in aerogel. *Annual Reviews of Earth and Planetary Science* 34:385–418.

Burchell M. J., Mann J., Creighton J. A., Kearsley A. T., Graham G., and Franchi I. A. 2006b. Identification of minerals and meteoritic materials via Raman techniques after capture in hypervelocity impacts on aerogel. *Meteoritics & Planetary Science* 41:217–232.

Burchell M. J., Fairey S. A. J., Wozniakiewicz P., Brownlee D. E., Hörz F., Kearsley A. T., See T., Tsou P., Warren J., Westphal A., Green S. F., Trigo-Rodríguez J. M., and Domínguez G. 2008. Characteristics of cometary dust tracks in Stardust aerogel and laboratory calibrations. *Meteoritics & Planetary Science* 43. This issue.

Domínguez G., Westphal A. J., Jones S. M., and Phillips M. L. F. 2004. Energy loss and impact cratering in aerogels: Theory and experiment. *Icarus* 172:613–624.

Flynn G., Bleuet P., Borg J., Bradley J. P., Brenker F., Brennan S., Bridges J. C., Brownlee D. E., Bullock E., Burghammer M., Clark B. C., Dai Z. R., Daghlian C. P., Djouadi Z., Fakra S., Ferroir T., Floss C., Franchi I. A., Gainsforth Z., Gallien J.-P., Gillet P., Grant P. G., Graham G. A., Grossemy F., Heck P., Herzog G. F., Hoppe P., Hörz F., Huth J., Igantyev K., Ishii H., Janssens K., Joswiak D., Kearsley A. T., Khodja H., Lanzirotti A., Leitner J., Lemelle L., Leroux H., Luening K.,

MacPherson G., Marhas K., Matrajt G., Nakamura T., Nakamura-Messenger K., Nakano T., Newville M., Papanastassiou D. A., Pianetta P., Rao W., Riekel C., Rietmeijer F., Rost D., Schwandt C. S., See T. H., Sheffield-Parker J. A., Simionovici S., Sitnitsky S. I., Snead C. J., Stadermann F. J., Stephan T., Stroud R. M., Susini J., Suzuki Y., Sutton S. R., Taylor S., Teslich N., Troadec D., Tsou P., Tsuchiyama A., Uesugi K., Vekemans B., Vicenzi E., Vincze L., Westphal A. J., Wozniakiewicz P. A., Zinner E., and Zolensky M. 2006. Elemental compositions of comet 81P/Wild 2 samples collected by Stardust. *Science* 314:1731–1735.

Hörz F., Cintala M. J., Zolensky M. E., Bernhard R. P., Davidson W. E., Haynes G., See T. H., Tsou P., and Brownlee D. E. 1998. Capture of hypervelocity particles with low-density aerogel. NASA TM-98-201792. 58 p.

Hörz F., Zolensky M. E., Bernhard R. P., See T. H., and Warren J. L. 2000. Impact features and projectile residues in aerogel exposed on Mir. *Icarus* 147:559–579.

Hörz F., Bastien R., Borg J., Bradley J. P., Bridges J. C., Brownlee D. E., Burchell M. J., Cintala M. J., Dai Z. R., Djouadi Z., Dominguez G., Economou T. E., Fairey S. A. J., Floss C., Franchi I. A., Graham G. A., Green S. F., Heck H., Hoppe P., Huth J., Ishii H., Kearsley A. T., Kissel J., Leitner J., Leroux H., Marhas M., Messenger K., Schwandt C. S., See T. H., Snead S., Stadermann F. J., Stephan T., Stroud R., Teslich N., Trigo-Rodríguez J. M., Tuzzolino A. J., Troadec D., Tsou P., Warren J., Westphal A., Wozniakiewicz P. J., Wright I., and Zinner E. 2006. Impact features on Stardust: Implications for comet Wild 2 dust. *Science* 314:1716–1719.

Kadono T. 1999. Hypervelocity impact into low-density material and cometary outburst. *Planetary and Space Science* 47:305–318.

Keller L. P., Bajt S., Baratta G. A., Borg J., Bradley J. P., Brownlee D. E., Busemann H., Brucato J. R., Burchell M., Colangeli L., D'Hendecourt L., Djouadi Z., Ferrini G., Flynn G., Franchi I. A., Fries M., Grady M. M., Graham G. A., Grossemy F., Kearsley A., Matrajt G., Nakamura-Messenger K., Mennella V., Nittler L., Palumbo M. E., Stadermann F. J., Tsou P., Rotundi A., Sandford S. A., Snead C., Steele A., Wooden D., and Zolensky Z. 2006. Infrared spectroscopy of comet 81P/Wild 2 samples returned by Stardust. *Science* 314:1728–1731.

Kitazawa Y., Fujiwara A., Kadono T., Imagawa K., Okada Y., and Uematsu K. 1999. Hypervelocity impact experiments on aerogel dust collector. *Journal of Geophysical Research* 104:22035–22052

Matrajt G., Wirick S., Ito M., Brownlee D., and Joswiak D. 2007. Carbon investigation of Stardust particles: A TEM, Nano-SIMS, and XANES study (abstract #1201). 38th Lunar and Planetary Science Conference. CD-ROM.

Melosh H. J. 1989. *Impact cratering: A geologic process*. Oxford: Oxford University Press. 245 p.

Noguchi T., Nakamura T., Okudaira K., Yano H., Sugita S., and Burchell M. J. 2007. Thermal alteration of hydrated minerals during hypervelocity capture to silica aerogel at the flyby speed of Stardust. *Meteoritics & Planetary Science* 42:357–372.

Öpik E. J. 1958. *Physics of meteor flight in the atmosphere*. New York: Interscience Publishers. 174 p.

Sandford S. A., Aléon J., Alexander C. M. O'D., Araki T., Bajt S., Baratta G. A., Borg J., Bradley J. P., Brownlee D. E., Brucato J. R., Burchell M. J., Busemann H., Butterworth A., Clemett S. J., Cody G., Colangeli L., Cooper G., D'Hendecourt L., Djouadi Z., Dworkin J. P., Ferrini G., Fleckenstein H., Flynn G. J., Franchi I. A., Fries M., Gilles M. K., Glavin D. P., Gounelle M., Grossemy F., Jacobsen C., Keller L. P., Kilcoyne A. L. D., Leitner J., Matrajt G., Meibom A., Mennella V., Mostefaoui S., Nittler L. R., Palumbo M. E., Papanastassiou D. A., Robert F., Rotundi A., Snead C. J., Spencer M. K., Stadermann F. J., Steele A., Stephan T., Tsou P., Tyliszczak T., Westphal A. J., Wirick S., Wopenka B., Yabuta H., Zare R. N., and Zolensky M. E. 2006. Organics captured from the comet Wild 2 by the Stardust spacecraft. *Science* 314:1720–1724.

Trigo-Rodríguez J. M. and Llorca J. 2006. Cometary meteoroids strength: Clues to the structure and evolution of comets. *Monthly Notices of the Royal Astronomical Society* 372:655–660.

Trigo-Rodríguez J. M. and Llorca J. 2007. Erratum: Cometary meteoroids strength: Clues to the structure and evolution of comets. *Monthly Notices of the Royal Astronomical Society* 375:415.

Trucano T. G. and Grady D. 1995. Impact shock and penetration fragmentation in porous media. *International Journal of Impact Engineering* 17:861–872.

Tsou P., Brownlee D. E., Laurance M. R., Hrubesh L., and Albee A. L. 1988. Intact capture of hypervelocity micrometeoroid analogs (abstract). 29th Lunar and Planetary Science Conference. pp. 1205–1206.

Tsou P., Brownlee D. E., Sandford S. A., Hörz F., and Zolensky M. E. 2003. Wild 2 and interstellar sample collection and Earth return. *Journal of Geophysical Research* 108:8113.

Zeldovich Y. B. and Raizer Y. P. 1966. *Physics of shock waves and high-temperature hydrodynamic phenomena,* 2002 edition. New York: Dover Publications. 944 p.

Zolensky M. E., Zega T. J., Yano H., Wirick S., Westphal A. J., Weisberg M. K., Weber I., Warren J. L., Velbel M. A., Tsuchiyama A., Tsou P., Toppani A., Tomioka N., Tomeoka K., Teslich N., Taheri M., Susini J., Stroud R., Stephan T., Stadermann F. J., Snead C. J., Simon S. B., Simionovici A., See T. H., Robert F., Rietmeijer F. J. M., Rao W., Perronnet M. C., Papanastassiou D. A., Okudaira K., Ohsumi K., Ohnishi I., Nakamura-Messenger K., Nakamura T., Mostefaoui S., Mikouch T., Meibom A., Matrajt G., Marcus M. A., Leroux H., Le Melle L., Le L., Lanzirotti A., Langenhorst F., Krot A. N., Keller L. P., Kearsley A. T., Joswiak D., Jacob D., Ishii H., Harvey R., Hagiya K., Grossman L., Grossman J. N., Graham G. A., Gounelle M., Gillet Ph., Genge M. J., Flynn G., Ferroir T., Fallon S., Ebel D. S., Dai Z. R., Cordier P., Clark B., Chi M., Butterworth A. L., Brownlee D. E., Bridges J. C., Brennan S., Brearley A., Bradley J. P., Bleuet P., Bland P. A., and Bastien R. 2006. Mineralogy and petrology of comet 81P/Wild 2 nucleus samples. *Science* 314:1735–1739.